Cell Selectivity and Mechanism of Action of Antimicrobial Model Peptides Containing Peptoid Residues†

Yun Mi Song,‡,§ Yoonkyung Park,‡,§ Shin Saeng Lim,‡ Sung-Tae Yang,|| Eun-Rhan Woo,‡ Il-Seon Park,‡ Jung Sup Lee,‡ Jae Il Kim,|| Kyung-Soo Hahm,‡ Yangmee Kim,⊥ and Song Yub Shin*,‡

Department of Bio-Materials, Graduate School and Research Center for Proteineous Materials, Chosun University, Gwangju 501-759, Korea, Department of Life Science, Gwangju Institute of Science and Technology, Gwangju 500-712, Korea, and Department of Chemistry, Konkuk University, Seoul 143-701, Korea

Received April 27, 2005; Revised Manuscript Received July 1, 2005

ABSTRACT: To develop a useful method for designing cell-selective antimicrobial peptides and to investigate the effect of incorporating peptoid residues into an α-helical model peptide on structure, function, and mode of action, we synthesized a series of model peptides incorporating Nala (Ala-peptoid) into different positions of an amphipathic α-helical model peptide (KLW). Incorporation of one or two Nala residues into the hydrophobic helix face of KLW was more effective at disrupting the α-helical structure and bacterial cell selectivity than incorporation into the hydrophilic helix face or hydrophobic/hydrophilic interface. Tryptophan fluorescence studies of peptide interaction with model membranes indicated that the cell selectivity of KLW-L9-*a* and KLW-L9,13-*a* is closely correlated with their selective interactions with negatively charged phospholipids. KLW-L9,13-*a*, which has two Nala residues in its hydrophobic helix face, showed a random structure in membrane-mimicking conditions. KLW-L9,13-*a* exhibited the highest selectivity toward bacterial cells, showing no hemolytic activity and no or less cytotoxicity compared with other peptides against four mammalian cell lines. Unlike other model peptides, KLW-L9,13-*a* caused no or little membrane depolarization in *Staphylococcus aureus* or lipid flip-flop in negatively charged vesicles. In addition, KLW-L9,13-*a* caused very little fluorescent dye leakage from negatively charged vesicles. Furthermore, confocal laser-scanning microscopy and DNA-binding assays showed that KLW-L9,13-*a* probably exerts its antibacterial action by penetrating the bacterial membrane and binding to cytoplasmic compounds (e.g., DNA), resulting in cell death. Collectively, our results demonstrate that the incorporation of two Nala residues into the central position of the hydrophobic helix face of noncell-selective α-helical peptides is a promising strategy for the rational design of intracellular, cell-selective antimicrobial peptides.

Antimicrobial peptides are widely distributed throughout the animal and plant kingdoms (*1*). They display a broad spectrum of antimicrobial activity against bacteria and yeast and are recognized as an important component of the innate immunity and host defense against microbial infections (*2*, *3*). The antimicrobial activity of these peptides is related to their ability to adopt amphipathic secondary structures, including α helices, β sheets, and β turns, in membrane-mimicking environments (*4*). The most abundant structural type in naturally occurring antimicrobial peptides is an amphipathic α helix (*5*). Their principal mode of antimicrobial action appears to involve depolarization or permeabilization of the bacterial cell membrane, although the detailed mechanisms are not fully understood (*6*−*8*). There are two classes of amphipathic α-helical antimicrobial peptides: cell-selective peptides (e.g., magainins and cecropins), which have potent activity against bacterial cells only, and noncell-selective peptides (e.g., melittin and pardaxin), which have lytic activity against both mammalian and bacterial cells. Many studies have focused on designing cell-selective peptides with strong antibacterial activity but no hemolytic activity (used as a measure of cytotoxicity in mammalian cells) for use as antibiotic drugs (*9*−*19*).

Proline is an α-helix-breaking amino acid because it lacks an amide proton and hence cannot form the intramolecular hydrogen bonds that are an essential feature of the α-helical structure. Despite this unfavorable property, a number of naturally occurring amphipathic α-helical antimicrobial peptides that promote ion-channel formation, such as cecropin A, melittin, pardaxin, and PMAP-23, contain either one or two proline residues near the middle of their sequences (*4*, *5*). Substitution of Pro by Ala in cell-selective α-helical antimicrobial peptides containing one or two prolines causes a significant increase in their hemolytic activity (*20*−*24*). In contrast, the incorporation of one or two prolines into

† This study was supported by grants from the Ministry of Science and Technology, Korea, the Korea Science and Engineering Foundation through the Research Center for Proteineous Materials, the Molecular and Cellular BioDiscovery Research Program of the Ministry of Science and Technology, Korea, and the National R&D Program for Fusion Strategy of Advanced Technologies of MOST, Korea.

* To whom correspondence should be addressed. Telephone: 82-62-230-6769. Fax: 82-62-227-8345. E-mail: syshin@chosun.ac.kr.

‡ Chosun University.

§ Yun Mi Song and Yoonkyung Park contributed equally to this work.

|| Gwangju Institute of Science and Technology.

⊥ Konkuk University.

10.1021/bi050765p CCC: $30.25
Published on Web 08/16/2005

Table 1: Amino Acid Sequences of KLW and Its Nala-Containing Peptides

peptide	sequence[a]	molecular mass (Da) calculated	molecular mass (Da) observed
KLW	KWKKLLKKLLKLLKKLLK-NH_2	2262.1	2262.3
KLW-L9-*a*	KWKKLLKK***a***LKLLKKLLK-NH_2	2220.0	2219.3
KLW-L10-*a*	KWKKLLKKL***a***KLLKKLLK-NH_2	2220.0	2219.2
KLW-K11-*a*	KWKKLLKKLL***a***LLKKLLK-NH_2	2205.0	2205.7
KLW-L9,13-*a*	KWKKLLKK***a***LKL***a***KKLLK-NH_2	2177.9	2178.7
KLW-K7,11-*a*	KWKKLL***a***KLL***a***LLKKLLK-NH_2	2147.9	2148.4

[a] ***a***, Nala (Ala-peptoid).

noncell-selective linear α-helical antimicrobial peptides lacking proline greatly reduces their hemolytic activity without affecting their antibacterial activity (*25*−*28*). These results suggest that the structural flexibility provided by one or two prolines in α-helical antimicrobial peptides plays an important role in the selectivity for bacterial versus mammalian cells.

Similar to Pro, peptoid residues are imino acids because their side chains are shifted from the α-carbon position to the N position. In addition, peptoid residues disrupt the stable α-helical structure of the peptide because of their lack of an amide proton (*29*). Therefore, we conjectured that incorporation of a peptoid residue into a linear noncell-selective α-helical antimicrobial peptide would improve the selectivity for bacterial versus mammalian cells. To our knowledge, the effect of peptoid residues on the structure, biological function, and mode of action of amphipathic α-helical antimicrobial peptides has not been previously examined. For this purpose, we synthesized a series of peptides wherein one or two Nala (Ala-peptoid) residues were replaced in the hydrophobic helix face, the hydrophobic/hydrophilic interface, or the hydrophilic helix face of a noncell-selective, amphipathic α-helical model peptide (KLW). We characterized the biological activity of these peptides using human erythrocytes, other mammalian cell types, and bacterial cells, and we examined their interaction with model phospholipid membranes by tryptophan fluorescence. Further, we examined the peptide secondary structures in membrane-mimicking environments by circular dichroism (CD)[1] spectroscopy, and we assessed their ability to cause membrane permeabilization, lipid flip-flop, and membrane depolarization. Finally, the sites of action and the molecular mechanisms of antimicrobial activity were investigated by confocal laser-scanning microscopy and DNA-binding assays. These Nala-containing peptides offer unique insights into the mode of interaction between peptides and model membranes or intact bacterial cells, and the results provide important information on the parameters that affect bacterial cell selectivity.

[1] Abbreviations: CD, circular dichroism; C_6-NBD-PC, 1-palmitoyl-2-[6-[7-nitrobenz-2-oxa-1,3-diazol-4-yl]amino]capryl]-L-α-phosphatidylcholine; CFU, colony-forming unit; $DiSC_3(5)$, 3,3′-dipropylthiadicarbocyanine iodide; DPC, dodecylphosphocholine; DTT, dithiothreitol; EYPC, egg yolk L-α-phosphatidylcholine; EYPE, egg yolk L-α-phosphatidylethanolamine; EYPG, egg yolk L-α-phosphatidyl-DL-glycerol; FITC, fluorescein isothiocyanate; h-RBC, human red blood cell; KCTC, Korean Collection for Type Cultures; LUV, large unilamellar vesicle; MIC, minimal inhibitory concentration; PBS, phosphate-buffered saline; RP-HPLC, reversed-phase high-performance liquid chromatography; SDS, sodium dodecyl sulfate; SRB, sulforhodamine B; SUV, small unilamellar vesicle; TFE, 2,2,2-trifluoroethanol; Tris, tris(hydroxymethyl)aminomethane.

MATERIALS AND METHODS

Materials. Rink amide 4-methylbenzhydrylamine resin, fluoren-9-yl-methoxycarbonyl (Fmoc)-amino acids, and other reagents for peptide synthesis were purchased from Calbiochem−Novabiochem (La Jolla, CA). Egg yolk L-α-phosphatidylcholine (EYPC), egg yolk L-α-phosphatidyl-DL-glycerol (EYPG), egg yolk L-α-phosphatidylethanolamine (EYPE), acrylamide, 2,2,2-trifluoroethanol (TFE), Tris (tris(hydroxymethyl)aminomethane), sodium dodecyl sulfate (SDS), calcein, trypsin, sodium dithionite, SRB (sulforhodamine B), and gramicidin D were obtained from Sigma Chemical Co. (St. Louis, MO). 3,3′-Dipropylthiadicarbocyanine iodide [$DiSC_3(5)$] was obtained from Molecular Probes (Eugene, OR). Dodecylphosphocholine (DPC) and 1-palmitoyl-2-[6-[7-nitrobenz-2-oxa-1,3-diazol-4-yl]amino]-capryl]-L-α-phosphatidylcholine (C_6-NBD-PC) were purchased from Avanti Polar Lipids (Alabaster, AL). All other reagents were of analytical grade. The buffers were prepared in double glass-distilled water.

Peptide Synthesis and Purification. The peptides and FITC-labeled peptides were prepared by the standard Fmoc-based solid-phase method on rink amide 4-methylbenzhydrylamine resin (0.54 mmol/g). The crude peptide was purified by preparative RPLC on a 15 μm C_{18} reverse-phase Shim-pack column (Shimadzu, Japan; 20 × 250 mm). The purified peptides were shown to be homogeneous (>98%) by analytical RP-HPLC on a 5 μm C_{18} reverse-phase Shim-pack column (Shimadzu, Japan; 4.6 × 250 mm). Matrix-assisted laser desorption/ionization time-of-flight mass spectrometry (MALDI−TOF MS; Shimadzu, Japan) was used to confirm their molecular weights (Table 1).

Antimicrobial Activity. The antimicrobial activities of the peptides were examined in sterile 96-well plates (Nunc F96 microtiter plates) in a final volume of 100 μL as follows (*12*, *14*). Aliquots (50 μL) of a bacterial suspension at 2×10^6 colony-forming units (CFU)/mL in culture medium (1% peptone) were added to 50 μL of aqueous peptide solution (serial 2-fold dilutions in 1% peptone). After incubation for 18−20 h at 37 °C, the inhibition of bacterial growth was determined by measuring the absorbance at 620 nm with a Microplate autoreader EL 800 (Bio-tek Instruments). The minimal inhibitory concentration (MIC) was defined as the lowest concentration of peptide that inhibited growth. Bacterial strains were purchased from the Korean Collection for Type Cultures (KCTC) at the Korea Research Institute of Bioscience and Biotechnology and included three types of Gram-positive bacteria (*Bacillus subtilis* [KCTC 3068], *Staphylococcus epidermidis* [KCTC 1917], and *Staphylococcus aureus* [KCTC 1621]) and three types of Gram-negative bacteria (*Escherichia coli* [KCTC 1682], *Pseudo-*

monas aeruginosa [KCTC 1637], and *Salmonella typhimurium* [KCTC 1926]).

Hemolytic Activity. Hemolytic activity of the peptides was tested against human red blood cells (h-RBCs) (*12*, *14*). Fresh h-RBCs were washed 3 times with phosphate-buffered saline (PBS; 35 mM phosphate buffer containing 150 mM NaCl at pH 7.4) by centrifugation for 10 min at 1000*g* and resuspended in PBS. The peptide solutions were then added to 50 μL of h-RBCs in PBS to give a final volume of 100 μL and a final erythrocyte concentration of 4%, v/v. The resulting suspension was incubated with agitation for 60 min at 37 °C. The samples were centrifuged at 1000*g* for 5 min. Release of hemoglobin was monitored by measuring the absorbance of the supernatant at 405 nm. Controls for no hemolysis (blank) and 100% hemolysis consisted of h-RBCs suspended in PBS and 0.1% Triton-X 100, respectively.

Cytotoxicity Assay. The cytotoxicity of the peptides against mammalian cells was determined using the sulforhodamine B (SRB) assay as previously described (*30*). A-549 (human nonsmall cell lung carcinoma), SK-OV-3 (human adenocarcinoma, ovary malignant ascites), SK-MEL-2 (human malignant melanoma, metastasis to skin of thigh), and NIH-3T3 (mouse fibroblast) were used in growth inhibitory activity assays. The cells were obtained from the Korea Research Institute of Chemical Technology (KRICT) (Daejon, Korea). Cells were seeded onto 96-well plates at a density of 2.0×10^4 cells/well in 180 μL of RPMI-1640 medium. The plates were then incubated at 37 °C for 24 h in a 5% CO_2 atmosphere, after which 20 μL of serially diluted peptide was added. The plates were incubated for a further 3 days, after which the medium was discarded and the cells were washed with 200 μL of cold PBS/well. The cells were then fixed by adding 50 μL of cold 50% aqueous trichloroactic acid (TCA) (4 °C for 30 min). The TCA was then discarded, and cells were washed 5 times with tap water and dried completely under an airflow hood at room temperature. The fixed cells were stained with 100 μL of sulforhodamine B (SRB) (0.4%, w/v, SRB in 1% aqueous acetic acid) for 30 min, after which they were washed with 1% aqueous acetic acid to remove unbound SRB. The plates were then air-dried, and 200 μL of 10 mM Tris buffer (pH 10.0) was added to dissolve bound dye. The absorbance at 520 nm was determined using an ELISA plate reader (Molecular Devices, Sunnyvale, CA). Wells in which cells were not treated with peptides were used as controls for cell viability, and wells without cells were used for "blanking" the spectrophotometer. The IC_{50} values represent the peptide dose causing a 50% reduction in absorbance compared to the absorbance observed in untreated control cell wells.

CD Spectra. The CD spectra of peptides were measured with a Jasco J-715 CD spectrophotometer (Tokyo, Japan) under nitrogen flush in 1-mm path-length cells at 25 °C. The spectra were recorded between 250 and 190 nm, and the average of four scans was taken. The percentage of α-helical structure was calculated as follows:

$$\%\ \alpha\text{-helical content} = ([\theta]_{222} - [\theta]^0_{222})/([\theta]^{100}_{222} - [\theta]^0_{222}) \times 100$$

where $[\theta]_{222}$ is the experimentally observed mean residue ellipticity at 222 nm and values for $[\theta]^0_{222}$ and $[\theta]^{100}_{222}$, which correspond to 0 and 100% helix content at 222 nm, are estimated to be −2000 and −32 000, respectively (*31*).

Peptide-Induced Dye Leakage from Liposomes. Calcein-entrapped large unilamellar vesicles (LUVs) composed of EYPE/EYPG (7:3, w/w) or EYPC were prepared by vortexing the dried lipid in dye buffer solution (70 mM calcein, 10 mM Tris, 150 mM NaCl, and 0.1 mM EDTA at pH 7.4). Untrapped calcein was removed by gel filtration on a Sephadex G-50 column. The leakage of calcein from the LUVs was monitored by measuring fluorescence intensity at an excitation wavelength of 490 nm and an emission wavelength of 520 nm on a model RF-5301PC spectrophotometer (Shimadzu, Kyoto, Japan). The measurements were performed at 25 °C. For determination of 100% dye release, 10% Triton-X 100 (20 μL) was added to dissolve the vesicles. The percentage of dye leakage caused by the peptides was calculated as follows:

$$\text{dye leakage (\%)} = 100 \times (F - F_0)/(F_t - F_0)$$

where F is the fluorescence intensity achieved by the peptides and F_0 and F_t are the fluorescence intensities without the peptides and with Triton X-100, respectively.

Tryptophan Fluorescence and Quenching Experiments. In the tryptophan fluorescence and quenching experiments, small unilamellar vesicles (SUVs) were used to minimize differential light-scattering effects (*32*, *33*). The tryptophan fluorescence measurements were taken with a model RF-5301PC spectrophotometer (Shimadzu, Kyoto, Japan). Each peptide (final concentration, 3 μM) was added to 3 mL of Tris buffer (10 mM Tris, 0.1 mM EDTA, and 150 mM NaCl at pH 7.4) containing 0.6 mM liposomes. Tryptophan residues of each peptide were excited at 280 nm, and emission spectra were recorded from 300 to 400 nm.

Acrylamide quenching experiments were carried out at an excitation wavelength of 295 nm (*34*, *35*). Trp fluorescence was quenched by the titration of acrylamide from a 4 M stock solution to a final concentration of 0.4 M in the presence of liposomes at a peptide/lipid molar ratio of 1:200. The quenching data were analyzed by a Stern−Volmer plot using the following equation:

$$F_0/F = 1 + K_{sv}[Q]$$

where F_0 is the fluorescence of the peptide in the absence of acrylamide, F is the fluorescence of the peptide in the presence of acrylamide, K_{sv} is the Stern−Volmer quenching constant, and $[Q]$ is the concentration of acrylamide.

Lipid Flip-Flop. The peptide-induced lipid flip-flop was detected as previously reported (*36*). NBD-labeled LUVs were generated from EYPG/EYPC (7:3, w/w) LUVs containing 0.5 mol % C_6-NBD-PC. The symmetrically labeled vesicles were mixed with 1 M sodium dithionite/1 M Tris ([lipid] = 8 mM; [dithionite] = 60 mM) and incubated for 15 min at 30 °C to produce inner leaflet-labeled vesicles. The vesicles were immediately separated from dithionite by gel filtration (Sephadex G-50, 1.5 × 30 cm column). The fraction of NBD lipids that had flopped during incubation in the absence or presence of the peptide was measured on the basis of fluorescence quenching by sodium dithionite. The asymmetrically NBD-labeled LUVs (2.0 mL) were incubated with or without the peptide for various periods at

30 °C. In the peptide-containing samples, 20 μL of a trypsin solution (5 mg/mL) was added to 2 mL samples and reacted for 1 min to hydrolyze the peptide. After addition of 20 μL of 1 M sodium dithionite/1 M Tris, NBD fluorescence was monitored using excitation and emission wavelengths of 460 and 530 nm, respectively. The percent flip-flop was calculated using the following equation:

$$\% \text{ flip-flop} = 100 \times (F_0 - F_P)/(F_0 - F_t)$$

where F_0, F_P, and F_t represent the fluorescence intensity in asymmetrically labeled unilamellar liposomes without the peptide, with the peptide, and with Triton X-100, respectively.

Membrane Depolarization Assay. The membrane depolarization activity of the peptides was determined using intact *S. aureus* cells and the membrane potential-sensitive fluorescent dye, $DiSC_3(5)$, as described by Friedrich et al. (*37*). *S. aureus* cells were collected in mid-logarithmic phase and resuspended in buffer (100 mM NaCl, 25 mM potassium phosphate, and 0.2% glucose at pH 7.4) at 4 °C and immediately placed on ice for fluorescence measurements. Therefore, cells at an optical density at 600 nm of 0.05 were mixed with 20 nM $DiSC_3(5)$ in a fluorescence cuvette. The fluorescence emission was monitored at 20 °C using a model RF-5301PC spectrophotometer (Shimadzu, Kyoto, Japan) at 670 nm (excitation at 650 nm). Full dissipation of the membrane potential was obtained by adding gramicidin D (final concentration, 0.2 nM). The membrane potential-dissipating activity of the peptides is expressed as follows:

$$\% \text{ inhibition} = 100\,[(F_p - F_0)/(F_g - F_0)]$$

where F_0 is the stable fluorescence value after addition of the $DiSC_3(5)$ dye, F_p is the fluorescence value 2 min after addition of the peptides, and F_g is the fluorescence signal after the addition of gramicidin D.

Confocal Laser-Scanning Microscopy. *E. coli* cells were grown on Luria broth−agar plates at 37 °C, collected from the plate with a sterile plate loop, and suspended in 20 mL of Luria broth. After incubation at 37 °C for 6 h, 20 mL of *E. coli* cells in the mid-logarithmic phase was harvested by centrifugation, washed with 10 mM PBS, and resuspended in 10 mL of the same medium. To immobilize *E. coli* cells on glass slides, poly-L-lysine-coated glass slides were immersed in 10 mM PBS containing 10^7 CFU/mL of *E. coli*. After 30 min, slides were rinsed with 10 mM PBS. Adequately diluted FITC-labeled peptides were then added to the slides, and the interaction between FITC-labeled peptides and cell walls was examined by confocal laser-scanning microscopy using an Olympus IX 70 confocal laser-scanning microscope (Japan). Fluorescent images were obtained with a 488-nm band-pass filter for excitation of FITC.

DNA-Binding Assay. Gel-retardation experiments were performed by mixing 100 ng of the plasmid DNA (pBluescript II SK^+) with increasing amounts of peptide in 20 μL of binding buffer (5% glycerol, 10 mM Tris-HCl at pH 8.0, 1 mM EDTA, 1 mM dithiothreitol, 20 mM KCl, and 50 μg/mL bovine serum albumin). The reaction mixtures were incubated at room temperature for 1 h. Subsequently, 4 μL of native loading buffer was added (10% Ficoll 400, 10 mM Tris-HCl at pH 7.5, 50 mM EDTA, 0.25% bromophenol blue, and 0.25% xylene cyanol), and a 20-μL aliquot was applied to a 1% agarose gel electrophoresis in 0.5× Tris borate-EDTA buffer (45 mM Tris-borate and 1 mM EDTA at pH 8.0) (*38*). The plasmid DNA used in this experiment was purified by CsCl-gradient ultracentrifugation to select the closed circular form of the plasmid.

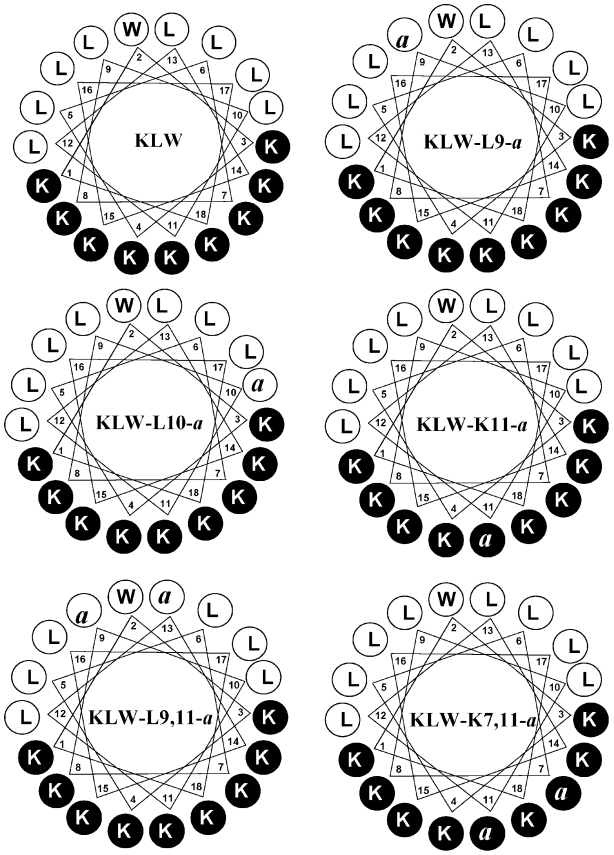

FIGURE 1: Schiff and Edmonson's wheel projection of KLW and its Nala-containing peptides. *a* = Nala (Ala-peptoid). Hydrophobic amino acids (Leu and Trp) are shown on a white background, and hydrophilic amino acids (Lys) are shown on a black background.

RESULTS

Peptide Design. A noncell-selective antimicrobial model peptide, KLW (Table 1), was designed to create a perfect amphipathic α-helical structure based on Schiff and Edmonson's wheel projection (Figure 1). On the basis of a regular α-helical structure of 3.6 residues per turn, a length of 18 residues was chosen so that five complete turns of an α helix were possible. KLW is composed of nine lysines, eight leucines, and one tryptophan, and the ratio of hydrophobic/hydrophilic residues is 1:1. One tryptophan was introduced to allow monitoring of peptide-membrane interactions. To investigate the function of the peptoid residue on the cell selectivity of the α-helical antimicrobial peptide, we designed and synthesized a series of model peptides containing one or two Nala residues in the hydrophobic helix face, hydrophobic/hydrophilic interface, or hydrophilic helix face of KLW (Table 1). In the one-Nala-containing peptides (KLW-L9-*a*, KLW-L10-*a*, and KLW-K11-*a*), Nala replaced Leu at position 9 of the hydrophobic helix face, Leu at position 10 of the hydrophobic/hydrophilic interface, or Lys at position 11 of the hydrophilic helix face (Figure 1). In the two-Nala-

Table 2: Minimal Inhibitory Concentration of the Peptides[a]

peptide	minimal inhibitory concentration (μM)					
	E. coli (KCTC1682)	*P. aeruginosa* (KCTC1637)	*S. typhimurium* (KCTC1926)	*B. subtilis* (KCTC3068)	*S. epidermidis* (KCTC1917)	*S. aureus* (KCTC1621)
KLW	4	4	4	8	4	4
KLW-L9-*a*	2	2	2	4	1	2
KLW-L10-*a*	4	4	4	4	2	4
KLW-K11-*a*	4	4	4	4	4	4
KLW-L9,13-*a*	2	2	2	4	1	2
KLW-K7,11-*a*	4	4	2	4	2	2

[a] Results represent the means of three independent experiments each performed in triplicate.

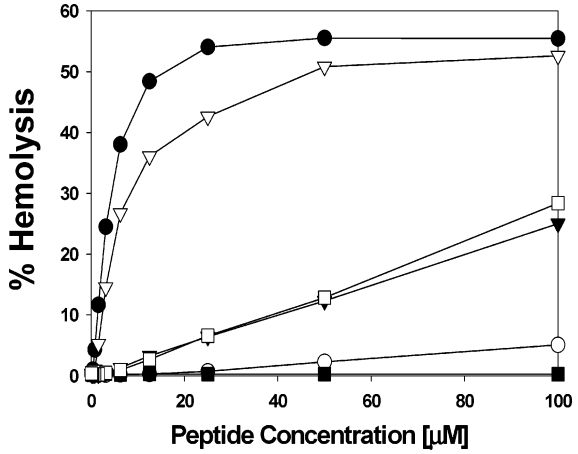

FIGURE 2: Dose−response curves of the hemolytic activity of the peptides toward human erythrocytes. Peptides are indicated as follows: (●) KLW, (○) KLW-L9-*a*, (▼) KLW-L10-*a*, (▽) KLW-K11-*a*, (■) KLW-L9,13-*a*, and (□) KLW-K7,11-*a*.

containing peptides (KLW-L9,13-*a* and KLW-K7,11-*a*), Nala replaced two Leu residues at positions 9 and 13 of the hydrophobic face or two Lys residues at positions 7 and 11 of the hydrophilic face (Figure 1). These substitution sites were also located near the central position of the overall peptide sequence. This was based on previous model peptide studies, demonstrating that substitutions at these central locations have the greatest effect on peptide secondary structure (*39*).

Antimicrobial and Hemolytic Activities of the Peptides. The antimicrobial activities of the peptides against three Gram-negative and three Gram-positive species of bacteria were determined by the broth microdilution method. The MIC values of the peptides are summarized in Table 2. KLW-L9-*a* and KLW-L9,13-*a* displayed a 2−4-fold higher antibacterial activity than KLW against all of the bacterial strains tested. In contrast, KLW-L10-*a*, KLW-K11-*a*, and KLW-K7,11-*a* displayed similar 2-fold higher activities compared to KLW. Figure 2 shows dose−response curves for the hemolytic activities of the peptides. Substitution of Nala for Leu^9 in the hydrophobic helix face of KLW (KLW-L9-*a*) results in much less hemolytic activity than when Lys^{11} in the hydrophilic helix face or Leu^{10} in the hydrophobic/hydrophilic interface is replaced. In addition, KLW-L9,13-*a*, which has two Nala residues in the hydrophobic helix face of KLW, displayed a much lower hemolytic activity than KLW-K7,11-*a*, which has two Nala residues in the hydrophilic helix face.

Peptide Cytotoxicity against Eukaryotic Cells. We examined the ability of the peptides to inhibit growth of eukaryotic cells derived from four tissue types: A-549, SK-OV-3, SK-MEL-2, and NIH-3T3. The resultant growth inhibition dose−response curves for the peptides are shown in Figure 3. The IC_{50} values refer to the peptide concentration causing 50% cell-growth inhibition compared to the growth of untreated control cells (Table 3). For all mammalian cells lines, the results showed that peptides other than KLW-L9,13-*a* were highly cytotoxic (IC_{50}, ∼0.6−7.1 μM). In contrast, KLW-L9,13-*a* showed either no toxicity or less toxicity than was observed for the other peptides (IC_{50}, from ∼31.9 to >100 μM).

Table 3: Cytotoxicity of the Peptides against Mammalian Cells

peptide	IC_{50} (μM)[a]			
	A-549	SK-OV-3	SK-MEL-2	NIH-3T3
KLW	0.6	0.6	0.7	1.8
KLW-L9-*a*	2.0	1.7	2.1	7.1
KLW-L10-*a*	1.0	0.9	1.3	2.0
KLW-K11-*a*	0.6	0.5	0.6	1.0
KLW-L9,13-*a*	75.5	31.9	38.7	>100
KLW-K7,11-*a*	1.0	0.7	1.1	2.0

[a] The IC_{50} values of the peptides were determined by the SRB method (*30*).

CD Spectroscopy. To investigate the secondary structure of the peptides in lipid membranes, the CD spectrum of each peptide was measured in various membrane-mimicking conditions (Figure 4). However, the CD spectra for all of the peptides in aqueous buffer displayed a negative band at approximately 200 nm, indicating that the structure is random. The CD spectrum for all of the peptides except for KLW-L9,13-*a* exhibited double-negative bands at 208 and 222 nm in the presence of 50% TFE, 30 mM SDS, or 50 mM DPC, suggesting that the peptides adopt a well-defined α-helical structure in lipid membranes. Table 4 shows the CD spectral data for the peptides in the presence of 50% TFE, 30 mM SDS, or 50 mM DPC, as well as their α helicities calculated from $[\theta]$ at 222 nm. The single-substituted peptides (KLW-L9-*a*, KLW-L10-*a*, and KLW-K11-*a*) and one of the double-substituted peptides (KLW-K7,11-*a*) displayed much lower α helicities than KLW. Interestingly, the CD spectrum for KLW-L9,13-*a* exhibited a strong negative band near 200 nm, indicating a disordered structure.

Tryptophan Fluorescence. One of the major differences between bacterial plasma and erythrocyte membranes is that the outer leaflets of erythrocyte membranes are almost exclusively composed of zwitterionic phospholipids, whereas bacterial membranes contain abundant negatively charged phospholipids (*40*, *41*). To determine the local environments of the peptides, we monitored the fluorescence emission of each tryptophan residue of the peptide in Tris buffer or in

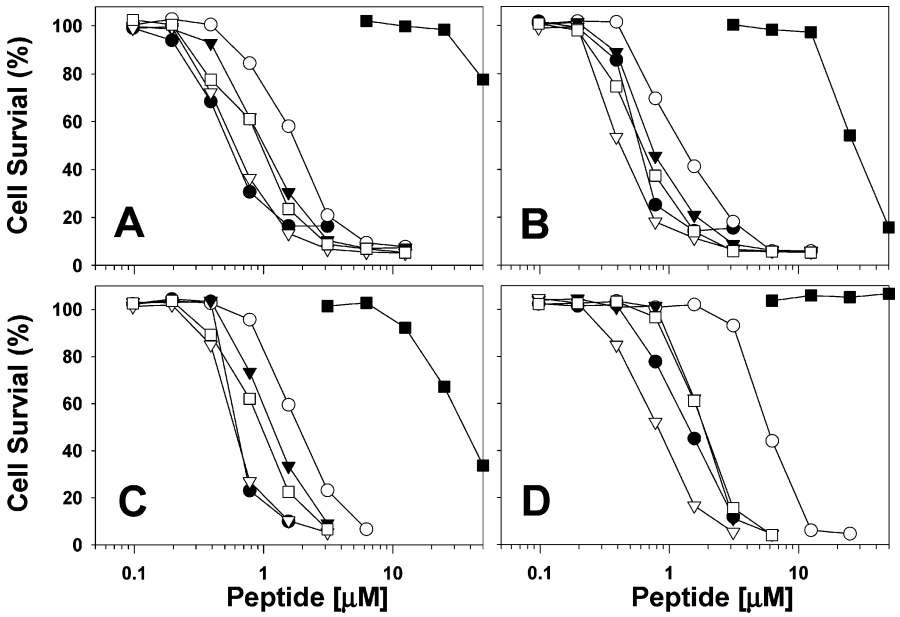

FIGURE 3: Growth inhibition dose−response curves for the peptides when incubated with four distinct mammalian cell lines: A-549 (A), SK-OV-3 (B), SK-MEL-2 (C), and NIH-3T3 (D). Cytotoxicity was assessed using the SRB assay. Peptides are indicated as follows: (●) KLW, (○) KLW-L9-*a*, (▼) KLW-L10-*a*, (▽) KLW-K11-*a*, (■) KLW-L9,13-*a*, and (□) KLW-K7,11-*a*.

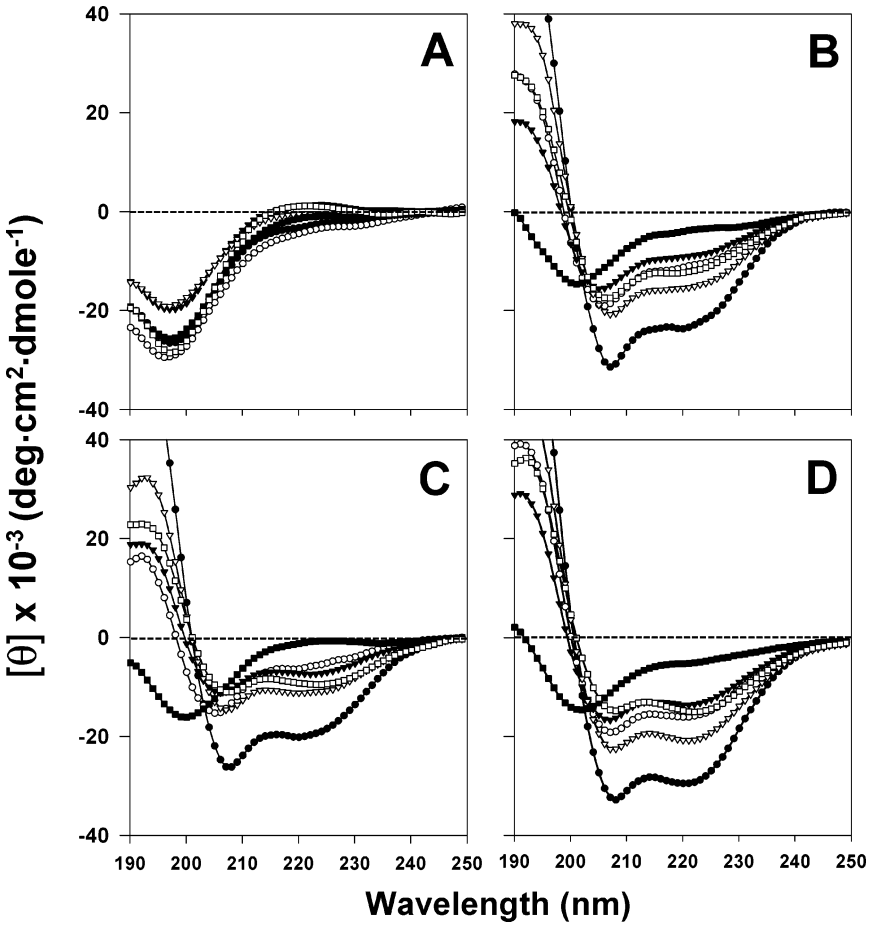

FIGURE 4: CD spectra of the peptides in sodium phosphate buffer at pH 7.4 (A) and buffer with 50% TFE (B), 30 mM SDS (C), or 50 mM DPC (D). Peptides are indicated as follows: (●) KLW, (○) KLW-L9-*a*, (▼) KLW-L10-*a*, (▽) KLW-K11-*a*, (■) KLW-L9,13-*a*, and (□) KLW-K7,11-*a*.

the presence of vesicles composed of either zwitterionic phospholipids (EYPC SUVs) or negatively charged phospholipids [EYPE/EYPG (7:3, w/w) SUVs]. In negatively charged vesicles, all peptides showed very similar large blue shifts in the emission maxima, suggesting that the Trp residue in all of the peptides inserts into the more hydrophobic environment of the membrane interior. In the zwitterionic phospholipid vesicles, there were significant blue shifts in the emission maxima for KLW, KLW-L10-*a*, KLW-K11-*a*, and KLW-K7,11-*a*, whereas there was no blue shift in the

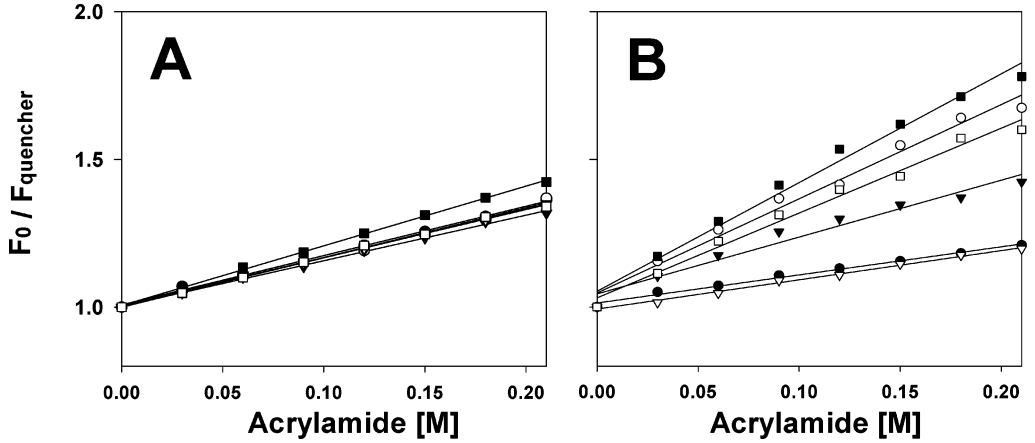

FIGURE 5: Stern−Volmer plots for the quenching of Trp fluorescence of the peptides by an aqueous quencher, acrylamide, in the presence of EYPE/EYPG (7:3, w/w) SUVs (A) and EYPC SUVs (B). Peptides are indicated as follows: (●) KLW, (○) KLW-L9-*a*, (▼) KLW-L10-*a*, (▽) KLW-K11-*a*, (■) KLW-L9,13-*a*, and (□) KLW-K7,11-*a*.

Table 4: Mean Residual Ellipticity at 222 nm ($[\theta]_{222}$) and Percent α-Helical Contents of the Peptides in 10 mM Sodium Phosphate Buffer (pH 7.4) Including 50% TFE (v/v), 30 mM SDS Micelles, or 50 mM DPC Micelles

	50% TFE (v/v)		30 mM SDS		50 mM DPC	
peptide	$[\theta]_{222}$	α helix (%)	$[\theta]_{222}$	α helix (%)	$[\theta]_{222}$	α helix (%)
KLW	−22 960.4	69.9	−19 772.8	59.2	−29 305.1	91.0
KLW-L9-*a*	−10 793.0	29.3	−5931.3	13.1	−15 841.6	46.1
KLW-L10-*a*	−8865.8	22.9	−7418.0	18.1	−13 533.7	38.4
KLW-K11-*a*	−15 144.8	43.8	−11 081.1	30.3	−20 737.2	62.5
KLW-L9,13-*a*	−3664.6	5.5	−900.9	0	−5112.4	10.4
KLW-K7,11-*a*	−11 966.7	35.2	−9466.2	24.9	−15 067.3	43.6

Table 5: Tryptophan Emission Maxima of the Peptides in Tris Buffer (pH 7.4) or in the Presence of EYPE/EYPG (7:3, w/w) and EYPC Vesicles

peptides	Tris buffer (nm)	EYPE/EYPG (7:3, w/w) (nm)	EYPC (nm)
KLW	344	331 (13)[a]	333 (11)[a]
KLW-L9-*a*	350	334 (16)	349 (1)
KLW-L10-*a*	350	331 (19)	332 (18)
KLW-K11-*a*	350	332 (18)	340 (10)
KLW-L9,13-*a*	350	339 (11)	350 (0)
KLW-K7,11-*a*	351	336 (15)	345 (5)

[a] Blue shift in emission maximum.

emission maximum for KLW-L9-*a* or KLW-L9,13-*a* (Table 5).

Tryptophan Fluorescence Quenching Studies. To determine the relative extent to which the Trp residues of the peptides were buried in the model membranes, we performed a fluorescence quenching experiment using the water-soluble fluorescence quencher, acrylamide. The Stern−Volmer plots for the quenching of tryptophan by acrylamide in the presence of lipid vesicles are depicted in Figure 5. The tryptophan fluorescence for all peptides was decreased in a concentration-dependent manner by the addition of acrylamide. The quenching of Trp fluorescence was less effective with EYPE/EYPG (7:3, w/w) SUVs than with EYPC SUVs, suggesting that the Trp residue of the peptides was buried more extensively in negatively charged phospholipid vesicles than in zwitterionic phospholipid vesicles. In negatively charged phospholipid vesicles, the peptides all showed similar slopes. In contrast, in zwitterionic phospholipid vesicles, KLW-L9-*a* and KLW-L9,13-*a* exhibited a higher slope than the other peptides, suggesting that the Trp residues

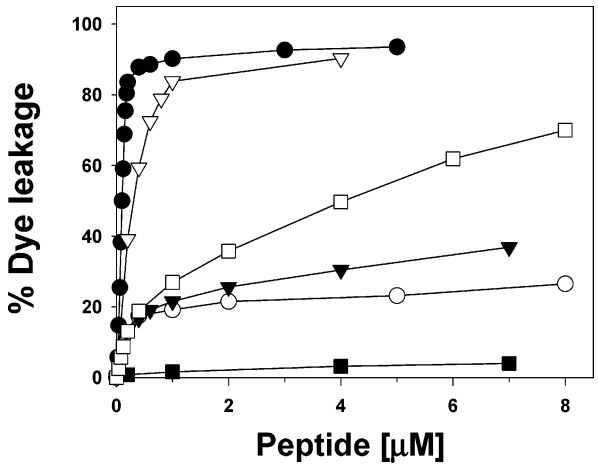

FIGURE 6: Percent leakage of calcein from negatively charged EYPE/EYPG (7:3, w/w) LUVs at pH 7.4, measured 2 min after the addition of the peptides. Peptides are indicated as follows: (●) KLW, (○) KLW-L9-*a*, (▼) KLW-L10-*a*, (▽) KLW-K11-*a*, (■) KLW-L9,13-*a*, and (□) KLW-K7,11-*a*.

of these peptides is less anchored within the hydrophobic core of the zwitterionic phospholipids compared to the other peptides.

Peptide-Induced Dye Leakage from Calcein-Loaded LUVs. We next studied the ability of the peptides to cause membrane leakage by testing their ability to evoke calcein release from LUVs made from negatively charged phospholipids. The percentage calcein leakage at 2 min after exposure to the peptide was used as a measure of membrane permeability. The dose−response curves of peptide-induced calcein release are shown in Figure 6. The order for the relative extent of calcein leakage from negatively charged vesicles of the peptides was KLW-L10-*a* ≅ KLW-K7,11-*a* ≅ KLW

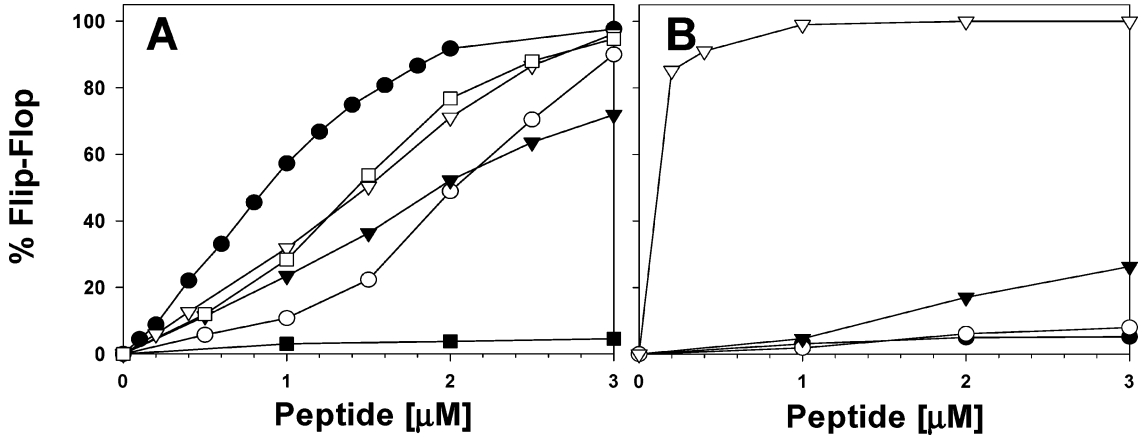

FIGURE 7: Percent flip-flop of the peptides in negatively charged EYPE/EYPG (7:3, w/w) LUVs. (A) (●) KLW, (○) KLW-L9-*a*, (▼) KLW-L10-*a*, (▽) KLW-K11-*a*, (■) KLW-L9,13-*a*, and (□) KLW-K7,11-*a*. (B) (●) Buforin II, (○) PR-39, (▼) magainin II, and (▽) melittin.

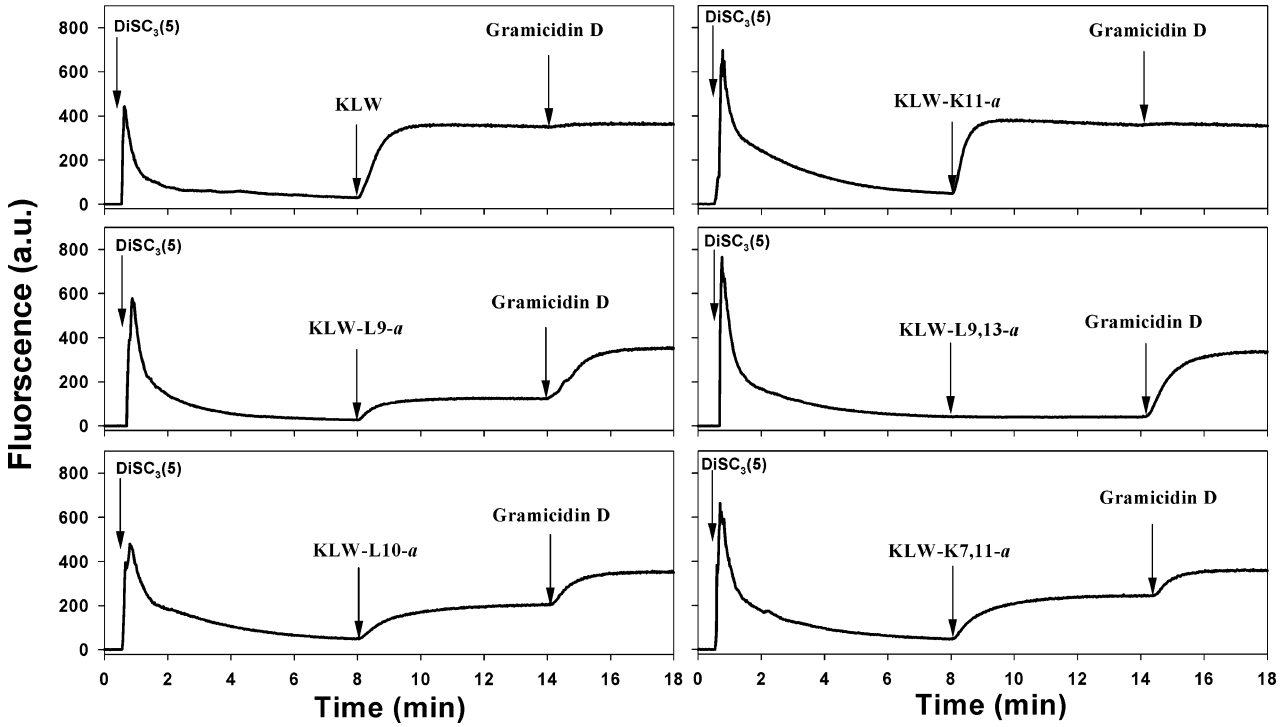

FIGURE 8: Effect of the peptides (peptide concentration, 0.1 μM) on the membrane potential of intact *S. aureus* cells (OD_{600} = 0.05). The fluorescence of the membrane potential-sensitive dye $DiSC_3(5)$ was measured as described in the Materials and Methods.

> KLW-K11-*a* > KLW-L9-*a* > KLW-L9,13-*a*. Interestingly, despite its potent antimicrobial activity, KLW-L9,13-*a* induced very little calcein release from negatively charged vesicles, even at a peptide concentration as high as 7 μM (Figure 5).

Lipid Flip-Flop. Similar to the positive control peptides, melittin and magainin II, all of the peptides except for KLW-L9,13-*a* induced a significant dose-dependent lipid flip-flop in EYPG/EYPE (7:3, w/w) LUVs. In contrast, similar to the negative control peptides buforin II and PR-39, KLW-L9,13-*a* showed no or little measurable lipid flip-flop, even at a peptide concentration as high as 3 μM (Figure 7).

Membrane Depolarization. The ability of the peptides to permeabilize the membranes of intact *S. aureus* cells was determined using the membrane potential-sensitive dye, $DiSC_3(5)$. This dye concentrates in the cytoplasmic membrane under the influence of the membrane potential, resulting in a self-quenching of fluorescence. Upon disruption of the membrane potential, the dye dissociates into the buffer, leading to an increase in fluorescence. As shown in Figure 8, the fluorescence intensity of $DiSC_3(5)$ was strongly quenched when this dye accumulated in the membrane interior of energized cells (first arrow). After a stable signal was observed, the peptides were added (second arrow). The membrane potential-dissipating activities of the peptides can be determined in relation to the effect of gramicidin D (third arrow), which fully collapses the membrane potential. The addition of 0.1 μM of all of the peptides except for KLW-L9,13-*a* caused a rapid increase in fluorescence because of a collapse of the ion gradients that generate the membrane potential. Dose−response curves of the membrane potential-dissipating activities of the peptides are shown in Figure 9. Furthermore, like buforin II and PR-39, which are known as intracellular-acting antimicrobial peptides, KLW-L9,13-*a* at the MIC (2 μM) did not cause a measurable dissipation of the potential (Figure 10).

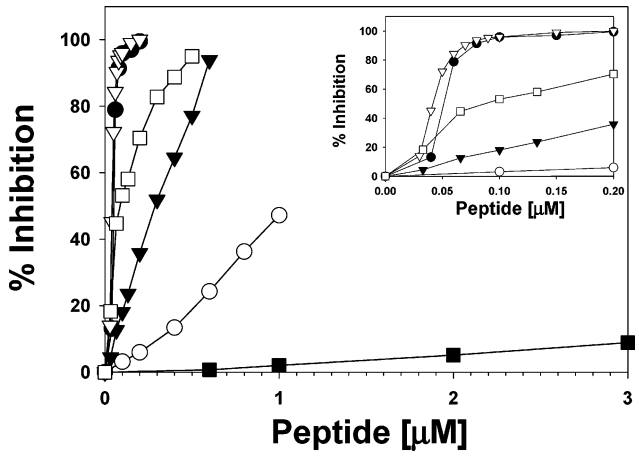

FIGURE 9: Dose−response curves of the membrane potential-dissipating activities of the peptides toward intact *S. aureus* cells (OD_{600} = 0.05). Peptides are indicated as follows: (●) KLW, (○) KLW-L9-*a*, (▼) KLW-L10-*a*, (▽) KLW-K11-*a*, (■) KLW-L9,13-*a*, and (□) KLW-K7,11-*a*.

Confocal Laser-Scanning Microscopy. To determine the site of action of the peptides, FITC-labeled peptides were incubated with *E. coli* and their localization was visualized by confocal laser-scanning microscopy. Figure 11 shows that, as observed for FITC-labeled buforin II, which is a cell-penetrating α-helical antimicrobial peptide, FITC-labeled KLW-L9,13-*a* (20 μg/mL) penetrated the bacterial cell membrane and accumulated in the cytoplasm. This finding indicates that the cytoplasm and not the membrane is the major site of action of KLW-L9,13-*a*. In contrast, under the same conditions, FITC-labeled KLW did not penetrate but remained associated with the cell membrane. The behavior of KLW was similar to that of magainin II, which is known as a noncell-penetrating peptide.

DNA-Binding Activity. We next examined the DNA-binding properties of the peptides to attempt to determine their molecular mechanisms of action. The DNA-binding affinities of the peptides were examined by analyzing the electrophoretic mobility of DNA bands at various peptide/DNA weight ratios. Similar to buforin II, KLW-L9,13-*a* inhibited the migration of DNA at concentrations above 12.5 μM. PR-39 suppressed the migration of DNA at concentrations above 25 μM. In contrast, KLW and melittin inhibited the migration of DNA at concentrations above 50 μM, and magainin II did not suppress the migration of DNA even at a concentration of 100 μM (Figure 12).

DISCUSSION

Peptoid residues have higher hydrophilicity, a greater likelihood of cis/trans isomerization, and more α-helix breaking potential than the corresponding amino acids because of the lack of the amide proton that forms hydrogen bonds with the α-helix backbone (*29*, *42*). Because of these specific properties of peptoid residues, the incorporation of a peptoid residue into a linear α-helical antimicrobial peptide is expected to impact its structure, cell selectivity, and interaction with lipid bilayers.

In the present study, we evaluated the structural and functional changes caused by the incorporation of Nala (Ala-peptoid) into a noncell-selective, ideal amphipathic α-helical antimicrobial model peptide (KLW). Specifically, we designed and synthesized a series of peptides in which one or two Nala were placed at the hydrophobic face, hydrophobic/hydrophilic interface, or hydrophilic face of KLW. To determine whether the peptides were selective for prokaryotic cells, we tested their hemolytic activity against highly susceptible human erythrocytes and their ability to inhibit the growth of four mammalian cell lines derived from different tissues (A-549, SK-OV-3, SK-MEL-2, and NIH-3T3). KLW-L9-*a* and KLW-L9,13-*a*, which have one and two Nala at the hydrophobic face, respectively, showed much higher bacterial cell selectivity than the peptides containing one or two Nala residues at the hydrophilic face or the hydrophobic/hydrophilic interface (KLW-L10-*a*, KLW-K11-*a*, and KLW-K9,13-*a*). In particular, KLW-L9,13-*a* showed the highest bacterial cell selectivity, with no hemolytic activity against human erythrocytes even at 100 μM (217.9 μg/mL), and either no or less cytotoxicity than other peptides in growth inhibitory assays using mammalian cells.

To understand the role of the lipid component and surface charge of bacterial and mammalian membranes in the cell selectivity of the peptide, we performed tryptophan fluorescence experiments in the presence of negatively charged EYPE/EYPG (7:3, w/w) vesicles or zwitterionic EYPC vesicles. It has been reported that noncell-selective antimicrobial peptides bind both to negatively charged and zwitterionic vesicles but that cell-selective antimicrobial peptides bind preferentially to negatively charged vesicles (*43*). We found that KLW-L9-*a* and KLW-L9,13-*a* permeabilized negatively charged EYPE/EYPG (7:3, w/w) vesicles more effectively than zwitterionic EYPC vesicles, suggesting that the greater selectivity of these peptides for bacterial cells is associated with their effective binding to negatively charged phospholipids.

Single-substituted peptides (KLW-L9-*a*, KLW-L10-*a*, and KLW-K11-*a*) showed typical α-helical conformations in the presence of 50% TFE, SDS micelles, or DPC micelles, which mimic cell-membrane environments, but they had much lower α helicity than KLW. The order of the percentage α-helical contents of the peptides was KLW-K11-*a* > KLW-L10-*a* > KLW-L9-*a*. The incorporation of one Nala residue into the hydrophobic face caused a more significant disruption of the α-helical structure of the peptide than incorporation into the hydrophobic/hydrophilic interface or hydrophilic helix face. These results indicate the importance of the hydrophobicity of the hydrophobic face in maintaining the α-helical structure.

Interestingly, unlike other Nala-containing model peptides, KLW-L9,13-*a*, which contains two Nala residues in the hydrophobic face, adopted a random structure in lipid-membrane-mimicking conditions, whereas KLW-K7,11-*a*, which contains two Nala residues in the hydrophilic face, retained an α-helical structure. Furthermore, KLW-L9,13-*a* showed strong antibacterial activity but no hemolytic activity. This result suggests that α helicity of the peptide is not required for antibacterial activity.

Two general mechanisms have been proposed to describe the process of phospholipid membrane permeation by the membrane-acting α-helical antimicrobial peptides (*44*). In the first, the barrel-stave model, amphipathic α helices insert into the hydrophobic core of the membrane and form transmembrane channels/pores. In the second, the carpet-like model, peptides that do not necessarily need to adopt

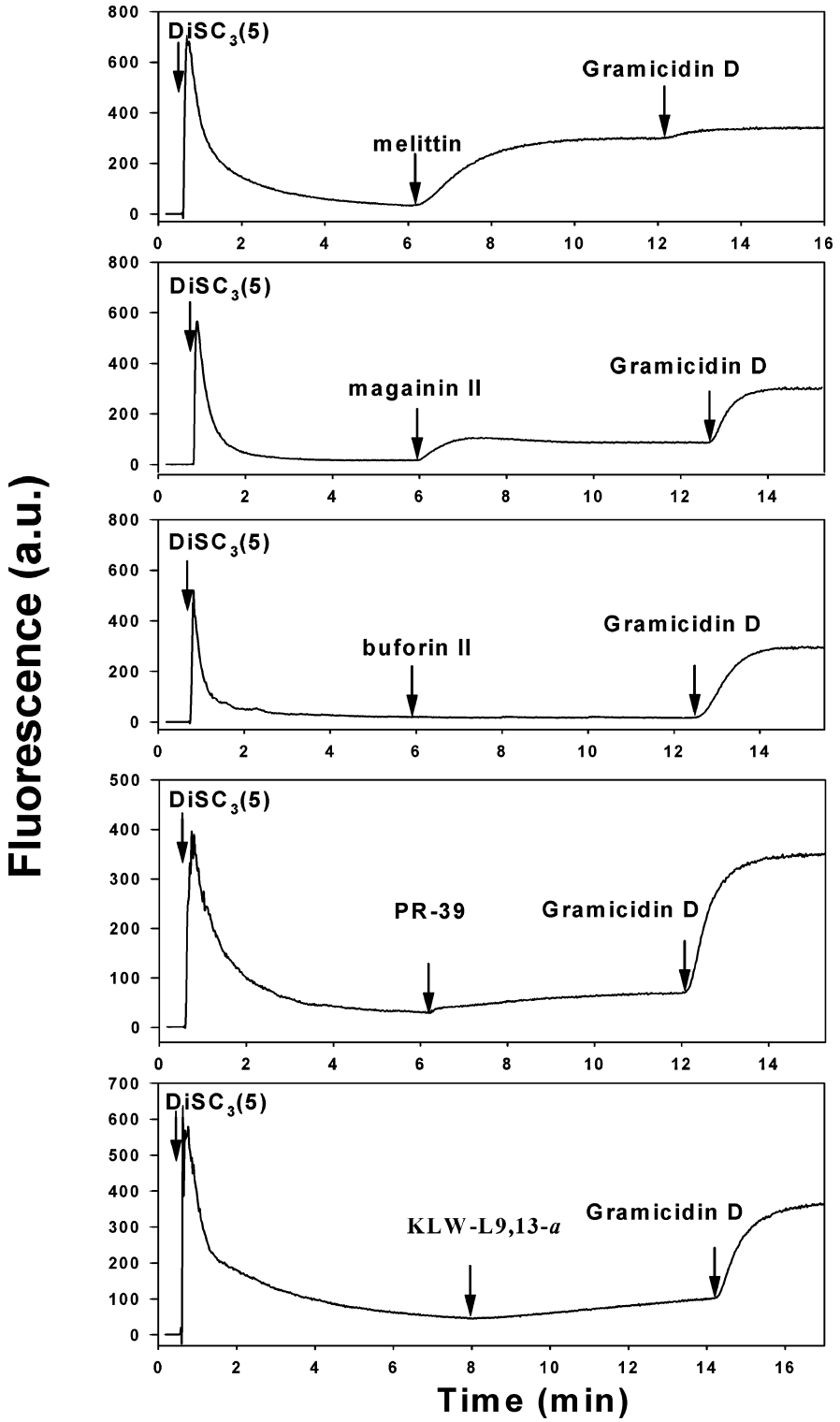

FIGURE 10: Effect of the peptides on the membrane potential of intact *S. aureus* cells ($OD_{600} = 0.05$). The fluorescence of the membrane potential-sensitive dye $DiSC_3(5)$ was measured as described in the Materials and Methods. Peptide concentrations were as follows: 0.1 μM melittin, 2 μM magainin II, 2 μM buforin II, 2 μM PR-39, and 2 μM KLW-L9,13-*a*.

an amphipathic α-helical structure are in contact with the lipid headgroup during the whole process of membrane permeation and do not insert into the hydrophobic core of the membrane. The specific permeation/disruption mechanism can vary among different peptides and could be due to a detergent-like disintegration or formation of toroidal pores or channel aggregates. For example, magainin II, a peptide isolated from the skin of the African clawed frog *Xenopus laevis*, forms a membrane-spanning pore composed of a dynamic, peptide-lipid supramolecular complex (toroidal pore) that mediates not only ion transport but also rapid flip-flop of the membrane lipids (*36*).

In contrast to these membrane-acting peptides, other classes of antimicrobial peptides have been suggested to target bacterial components other than membranes. Buforin II, discovered in the stomach tissue of the Asian toad *Bufo bufo gargarizans*, is one example. Buforin II is known to inhibit the macromolecular synthesis by penetration into the

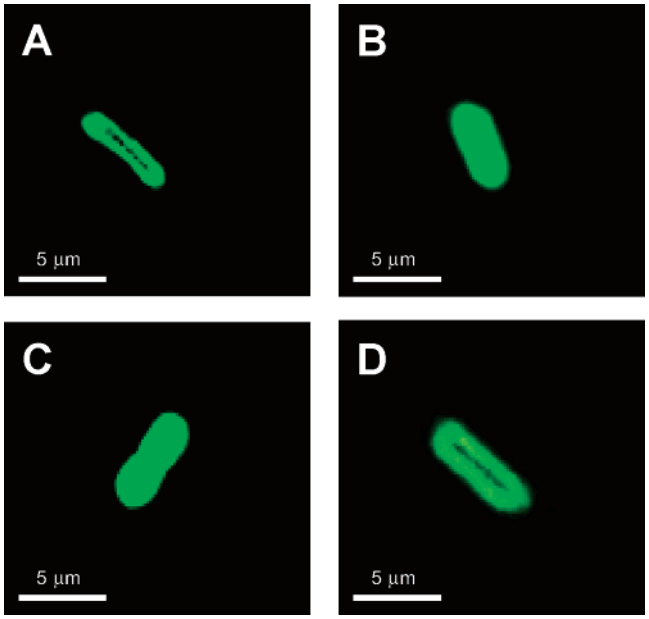

FIGURE 11: Confocal laser-scanning microscopy images of *E. coli* treated with FITC-labeled peptides. The immobilized cell was then reacted with 20 μg/mL FITC-labeled KLW (A), FITC-labeled KLW-L9,13-*a* (B), FITC-labeled buforin II (C), and FITC-labeled magainin II (D).

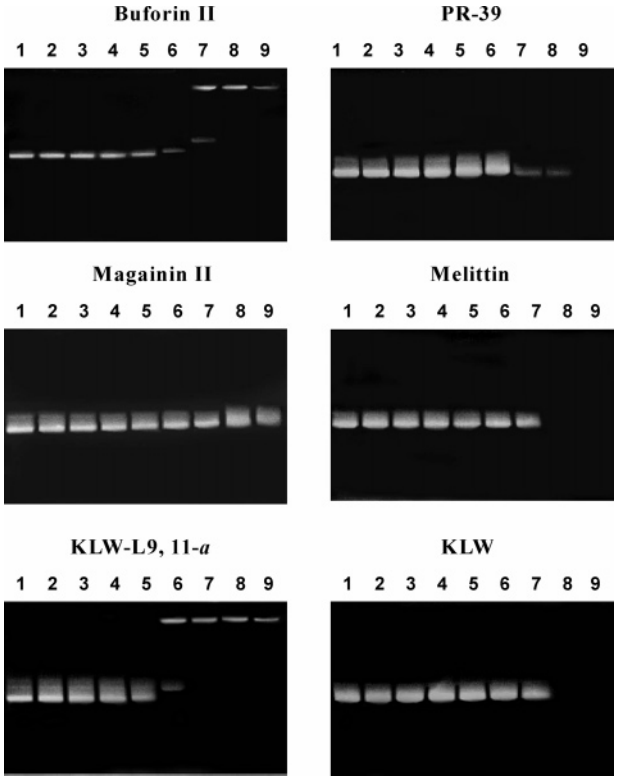

FIGURE 12: Interaction of the peptides with plasmid DNA. Binding was assayed by measuring the inhibition of migration by plasmid DNA (100 ng; pBluescript II SK^+). Lane 1, plasmid DNA alone; lane 2, 0.78 μM peptide; lane 3, 1.56 μM peptide; lane 4, 3.13 μM peptide; lane 5, 6.25 μM peptide; lane 6, 12.5 μM peptide; lane 7, 25 μM peptide; lane 8, 50 μM peptide; and lane 9, 100 μM peptide. DNA and the peptides were co-incubated for 1 h at room temperature before electrophoresis on a 1.0% agarose gel.

bacterial cytoplasm followed by DNA/RNA binding in the absence of severe membrane permeabilization or lipid flip-flop (*38*, *45*, *46*). Recently, buforin II was reported to cross the membrane via a mechanism similar to that of magainin II (i.e., pore formation), and the extremely short lifetime of the pore allows the peptide to translocate without membrane permeabilization (*47*).

To determine whether the bacterial membrane is the target of the Nala-containing model peptides, we tested the ability of the peptides to cause leakage of a fluorescent dye trapped within LUVs composed of negatively charged phospholipids. Despite effective binding and insertion into negatively charged phospholipids, as demonstrated by tryptophan fluorescence experiments, KLW-L9,13-*a* induced little dye leakage from negatively charged phospholipid vesicles even at the highest concentration tested (7 μM).

The ability of the peptides to depolarize the cytoplasmic membrane of the Gram-positive bacterium, *S. aureus*, was examined using the membrane potential-sensitive fluorescent dye $DiSC_3(5)$. This dye inserts into the cytoplasmic membrane under the influence of the membrane-potential gradient and quenches its own fluorescence. If the peptide forms a channel or otherwise disrupts the membrane, the membrane potential will be dissipated and the dye will be released into the medium, causing the fluorescence to increase. Similar to buforin II and PR-39, KLW-L9,13-*a* induced little or no measurable dissipation of the membrane potential at the MIC (3 μM). In contrast, as observed for magainin II and melittin, the other KLW model peptides caused a significant membrane depolarization even at concentrations as low as 0.1 μM. Furthermore, like magainin II, all of the Nala-containing model peptides except for KLW-L9,13-*a* induced significant dose-dependent lipid flip-flop. However, like buforin II, KLW-L9,13-*a* did not induce lipid flip-flop even at a concentration of 3 μM, suggesting that the antimicrobial action of KLW-L9,13-*a* is not due to the formation of pores or disintegration of the cell membrane.

Furthermore, to determine whether KLW-L9,13-*a* penetrates bacterial cell membranes and binds effectively to DNA, we carried out confocal laser-scanning microscopy using FITC-labeled peptides and DNA-binding assays. Similar to FITC-labeled buforin II, FITC-labeled KLW-L9,-13-*a* penetrated the cell membrane and accumulated in the cytoplasm, whereas FITC-labeled KLW and FITC-labeled magainin II did not penetrate the cell membrane. Furthermore, in the gel-retardation experiment, we confirmed that, like buforin II, KLW-L9,13-*a* has a higher affinity for DNA than magainin II. These results suggest that KLW-L9,13-*a* inhibits cellular functions by penetrating the bacterial cell membranes and binding to DNA, resulting in cell death.

In conclusion, we found that incorporation of one or two Nala residues into the hydrophobic face of a noncell-selective amphipathic α-helical model peptide, KLW, confers improved bacterial cell selectivity. Among the Nala-containing model peptides, KLW-L9,13-*a* showed the highest bacterial cell selectivity. Similar to buforin II, KLW-L9,13-*a* translocated effectively across lipid bilayers without causing membrane permeabilization or lipid flip-flop and bound strongly to DNA. These results suggest that KLW-L9,13-*a* probably exerts its antibacterial action by penetrating the bacterial membrane and binding to cytoplasmic compounds (e.g., DNA), resulting in cell death.

Collectively, our results demonstrate that novel peptides with an intracellular mechanism of action and high selectivity for bacterial cells can be generated by incorporation of two

Nala residues into the central position of the hydrophobic helix face of noncell-selective α-helical cytolytic peptides.

REFERENCES

1. Zasloff, M. (2002) Antimicrobial peptides of multicellular organisms, *Nature 415*, 389−395.
2. Hancock, R. E., and Scott, M. G. (2000) The role of antimicrobial peptides in animal defenses, *Proc. Natl. Acad. Sci. U.S.A. 97*, 8856−8861.
3. Hancock, R. E., and Diamond, G. (2000) The role of cationic antimicrobial peptides in innate host defences, *Trends Microbiol. 8*, 402−410.
4. Andreu, D., and Rivas, L. (1998) Animal antimicrobial peptides: An overview, *Biopolymers 47*, 415−433.
5. Tossi, A., Sandri, L., and Giangaspero, A. (2000) Amphipathic, α-helical antimicrobial peptides, *Biopolymers 55*, 4−30.
6. Oren, Z., and Shai, Y. (1998) Mode of action of linear amphipathic α-helical antimicrobial peptides, *Biopolymers 47*, 451−463.
7. Epand, R. M., and Vogel, H. J. (1999) Diversity of antimicrobial peptides and their mechanisms of action, *Biochim. Biophys. Acta 1462*, 11−28.
8. Epand, R. M., Shai, Y., Segrest, J. P., and Anantharamaiah, G. M. (1995) Mechanisms for the modulation of membrane bilayer properties by amphipathic helical peptides, *Biopolymers 37*, 319−338.
9. Shai, Y., and Oren, Z. (1996) Diastereomer of cytolysins, a novel class of potent antimicrobial peptides, *J. Biol. Chem. 271*, 7305−7308.
10. Oren, Z., Hong. J., and Shai Y. (1997) A repertoire of novel antimicrobial diastereomer peptides with selective cytolytic activity, *J. Biol. Chem. 272*, 14643−14649.
11. Hong. J., Oren, Z., and Shai Y. (1999) Structure and organization of hemolytic and nonhemolytic diastereomers of antimicrobial peptides in membranes, *Biochemistry 38*, 16963−16973.
12. Shin, S. Y., Kang, S. W., Lee, D. G., Eom, S. H., Song, W. K., and Kim, J. I. (2000) CRAMP analogues having potent antibiotic activity against bacterial, fungal, and tumor cells without hemolytic activity, *Biochem. Biophys. Res. Commun. 275*, 904−909.
13. Oh, J. E., and Lee, K. H. (2000) Characterization of the unique function of a reduced amide bond in a cytolytic peptide that acts on phospholipid membranes, *Biochem. J. 352*, 659−666.
14. Shin, S. Y., Lee, S. H., Yang, S.-T., Park, E. J., Lee, D. G., Lee, M. K., Eom, S. H., Song, W. K., Kim, Y., Hahm, K.-S., and Kim, J. I. (2001) Antibacterial, antitumor, and hemolytic activities of α-helical antibiotic peptide, P18 and its analogs, *J. Pept. Res. 58*, 504−514.
15. Dathe, M., Meyer, J., Beyermann, M., Maul, B., Hoischen, C., and Bienert, M. (2002) General aspects of peptide selectivity towards lipid bilayers and cell membranes studied by variation of the structural parameters of amphipathic α-helical model peptides, *Biochim. Biophys. Acta 1558*, 171−186.
16. Papo, N., Oren, Z., Pag, U., Sahl, H. G., and Shai, Y. (2002) The consequence of sequence alteration of an amphipathic α-helical antimicrobial peptide and its diastereomers, *J. Biol. Chem. 277*, 33913−33921.
17. Yan, H., Li, S., Sun, X., Mi, H., and He, B. (2003) Individual substitution analogs of Mel(12−26), melittin's C-terminal 15-residue peptide: Their antimicrobial and hemolytic actions, *FEBS Lett. 554*, 100−104.
18. Papo, N., and Shai, Y. (2004) Effect of drastic sequence alteration and D-amino acid incorporation on the membrane binding behavior of lytic peptides, *Biochemistry 43*, 6393−6403.
19. Chen, Y., Mant, C. T., Farmer, S. W., Hancock, R. E., Vasil, M. L., and Hodges, R. S. (2005) Rational design of α-helical antimicrobial peptides with enhanced activities and specificity/therapeutic index, *J. Biol. Chem. 280*, 12316−12329.
20. Thennarasu, S., and Nagaraj, R. (1996) Specific antimicrobial and hemolytic activities of 18-residue peptides derived from the amino terminal region of the toxin pardaxin, *Protein Eng. 9*, 1219−1224.
21. Suh, J. Y., Lee, Y. T., Park, C. B., Lee, K. H., Kim, S. C., and Choi, B. S. (1999) Structural and functional implications of a proline residue in the antimicrobial peptide gaegurin, *Eur. J. Biochem. 266*, 665−674.
22. Shin, S. Y., Park, E. J., Yang, S. T., Jung, H. J., Eom, S. H., Song, W. K., Kim, Y., and Hahm, K.-S., and Kim, J. I. (2001) Structure−activity analysis of SMAP-29, a sheep leukocytes-derived antimicrobial peptide, *Biochem. Biophys. Res. Commun. 285*, 1046−1051.
23. Park, K., Oh, D., Shin, S. Y., and Hahm, K.-S., and Kim, Y. (2002) Structural studies of porcine myeloid antibacterial peptide PMAP-23 and its analogues in DPC micelles by NMR spectroscopy, *Biochem. Biophys. Res. Commun. 290*, 204−212.
24. Pukala, T. L., Brinkworth, C. S., Carver, J. A., and Bowie, J. H. (2004) Investigating the importance of the flexible hinge in caerin 1.1: Solution structures and activity of two synthetically modified caerin peptides, *Biochemistry 43*, 937−944.
25. Zhang, L., Benz, R., and Hancock, R. E. (1999) Influence of proline residues on the antibacterial and synergistic activities of α-helical peptides, *Biochemistry 38*, 8102−8111.
26. Oh, D., Shin, S. Y., Lee, S., Kang, J. H., Kim, S. D., Ryu, P. D., and Hahm, K.-S., and Kim, Y. (2000) Role of the hinge region and the tryptophan residue in the synthetic antimicrobial peptides, cecropin A(1−8)-magainin 2(1−12) and its analogues, on their antibiotic activities and structures, *Biochemistry 39*, 11855−11864.
27. Song, Y. M., Yang, S. T., Lim, S. S., Kim, Y., Hahm, K.-S., Kim, J. I., and Shin, S. Y. (2004) Effects of L- or D-Pro incorporation into hydrophobic or hydrophilic helix face of amphipathic α-helical model peptide on structure and cell selectivity, *Biochem. Biophys. Res. Commun. 314*, 615−621.
28. Lee, K., Shin, S. Y., Kim, K., Lim, S. S., Hahm, K.-S., and Kim, Y. (2004) Antibiotic activity and structural analysis of the scorpion-derived antimicrobial peptide IsCT and its analogs, *Biochem. Biophys. Res. Commun. 323*, 712−719.
29. Tang, Y. C., and Deber, C. M. (2002) Hydrophobicity and helicity of membrane-interactive peptides containing peptoid residues, *Biopolymers 65*, 254−262.
30. Skehan, P., Storeng, R., Scudiero, D., Monks, A., McMahon, J., Vistica, D., Warren, J., Bokesch, H., Kenney, S., and Boyd, M. R. (1990) New colorimetric cytotoxicity assay for anticancer-drug screening. *J. Natl. Cancer Inst. 82*, 1107−1112.
31. Wu, C. S., Ikeda, K., and Yang, J. T. (1981) Ordered conformation of polypeptides and proteins in acidic dodecyl sulfate solution, *Biochemistry 20*, 566−570.
32. Mao, D., and Wallace, B. A. (1984) Differential light scattering and absorption flattening optical effects are minimal in the circular dichroism spectra of small unilamellar vesicles, *Biochemistry 23*, 2667−2673.
33. Shai, Y., Bachm, D., and Yanovsky, A. (1990) Channel formation properties of synthetic pardaxin and analogues, *J. Biol. Chem. 265*, 20202−20209.
34. De Kroon, A. I., Soekarjo, M. W., De Gier, J., and De Kruijff, B. (1990) The role of charge and hydrophobicity in peptide−lipid interaction: A comparative study based on tryptophan fluorescence measurements combined with the use of aqueous and hydrophobic quenchers, *Biochemistry 29*, 8229−8240.
35. Zhao, H., and Kinnunen, P. K. (2002) Binding of the antimicrobial peptide temporin L to liposomes assessed by Trp fluorescence, *J. Biol. Chem. 277*, 25170−25177.
36. Matsuzaki, K., Murase, O., Fujii, N., and Miyajima, K. (1996) An antimicrobial peptide, magainin 2, induced rapid flip-flop of phospholipids coupled with pore formation and peptide translocation, *Biochemistry 35*, 11361−11368
37. Friedrich, C. L., Moyles, D., Beveridge, T. J., and Hancock, R. E. (2000) Antibacterial action of structurally diverse cationic peptides on Gram-positive bacteria, *Antimicrob. Agents Chemother. 44*, 2086−2092.
38. Park, C. B., Kim, H. S., and Kim, S. C. (1998) Mechanism of action of the antimicrobial peptide buforin II: Buforin II kills microorganisms by penetrating the cell membrane and inhibiting cellular functions, *Biochem. Biophys. Res. Commun. 244*, 253−257.
39. Chen, Y., Mant, C. T., and Hodges, R. S. (2002) Determination of stereochemistry stability coefficients of amino acid side-chains in an amphipathic α-helix, *J. Pept. Res. 59*, 18−33.
40. Verkleij, A. J., Zwaal, R. F., Roelofsen, B., Comfurius, P., Kastelijn, D., and van Deenen, L. L. (1973) The asymmetric distribution of phospholipids in the human red cell membrane. A combined study using phospholipases and freeze-etch electron microscopy, *Biochim. Biophys. Acta 323*, 178−193.
41. Shaw, N. (1974) Lipid composition as a guide to the classification of bacteria, *Adv. Appl. Microbiol. 17*, 63−108.
42. Tang, Y. C., and Deber, C. M. (2004) Aqueous solubility and membrane interactions of hydrophobic peptides with peptoid tags, *Biopolymers 76*, 110−118.

43. Papo, N., and Shai, Y. (2003) Can we predict biological activity of antimicrobial peptides from their interactions with model phospholipid membranes? *Peptides 24*, 1693−1703.
44. Shai, Y., and Oren, Z. (2001) From "carpet" mechanism to *de novo* designed diastereomeric cell-selective antimicrobial peptides, *Peptides 22*, 1629−1641.
45. Park, C. B., Yi, K. S., Matsuzaki, K., Kim, M. S., and Kim, S. C. (2000) Structure−activity analysis of buforin II, a histone H2A-derived antimicrobial peptide: The proline hinge is responsible for the cell-penetrating ability of buforin II, *Proc. Natl. Acad. Sci. U.S.A. 97*, 8245−8250.
46. Kobayashi, S., Takeshima, K., Park, C. B., and Kim, S. C., and Matsuzaki, K. (2000) Interactions of the novel antimicrobial peptide buforin 2 with lipid bilayers: Proline as a translocation promoting factor, *Biochemistry 39*, 8648−8654.
47. Kobayashi, S., Chikushi, A., Tougu, S., Imura, Y., Nishida, M., Yano, Y., and Matsuzaki, K. (2004) Membrane translocation mechanism of the antimicrobial peptide buforin 2, *Biochemistry 43*, 15610−15616.

BI050765P